Construction and performance analysis of local DtN absorbing boundary conditions for exterior Helmholtz problems. Part I : Elliptical shaped boundaries

Hélène Barucq, Rabia Djellouli, Anne-Gaëlle Saint-Guirons

INRIA

INSTITUT NATIONAL DE RECHERCHE EN INFORMATIQUE ET EN AUTOMATIQUE

Construction and performance analysis of local *DtN absorbing boundary conditions for exterior Helmholtz problems. Part I : Elliptical shaped boundaries*

Hélène Barucq — Rabia Djellouli — Anne-Gaëlle Saint-Guirons

N° ????

October 2007

Thème NUM

ISSN 0249-6399 ISRN INRIA/RR--????--FR+ENG

Construction and performance analysis of *local* DtN absorbing boundary conditions for exterior Helmholtz problems. Part I : Elliptical shaped boundaries

Hélène Barucq * , Rabia Djellouli† , Anne-Gaëlle Saint-Guirons*

Thème NUM — Systèmes numériques
Projet Magique 3D

Rapport de recherche n° ???? — October 2007 — 30 pages

Abstract: We propose a new class of approximate *local* DtN boundary conditions to be applied on prolate spheroid-shaped exterior boundaries when solving acoustic scattering problems by elongated obstacles. These conditions are : (a) exact for the first modes, (b) easy to implement and to parallelize, (c) compatible with the local structure of the computational finite element scheme, and (d) applicable to exterior elliptical-shaped boundaries that are more suitable in terms of cost-effectiveness for surrounding elongated scatterers. Moreover, these conditions coincide with the classical local DtN condition designed for spherical-shaped boundaries. We investigate analytically and numerically the effect of the frequency regime and the slenderness of the boundary on the accuracy of these conditions when applied for solving radiators and scattering problems. We also compare their performance to the second order absorbing boundary condition (BGT2) designed by Bayliss, Gunzburger and Turkel when expressed in prolate spheroidal coordinates. The analysis reveals that, in the low frequency regime, the new second order DtN condition (DtN2) retains a good level of accuracy *regardless* of the slenderness of the boundary. In addition, the DtN2 boundary condition outperforms the BGT2 condition. Such superiority is clearly noticeable for large eccentricity values.

Key-words: Absorbing boundary conditions, elliptical coordinates, Dirichlet-to-Neumann operator, scattering problems

* Laboratoire de Mathématiques Appliquées, CNRS UMR 5142, Université de Pau et des Pays de l'Adour, IPRA-Avenue de l'Université, 64013 Pau, France
† Department of Mathematics, California State University Northridge, CA 91330-8313, USA

Unité de recherche INRIA Futurs
Parc Club Orsay Université, ZAC des Vignes,
4, rue Jacques Monod, 91893 ORSAY Cedex (France)
Téléphone : +33 1 72 92 59 00 — Télécopie : +33 1 60 19 66 08

Construction et analyse de performance de contidions aux limites absorbantes de type DtN localisé pour des problèmes extérieurs d'Helmholtz. Partie I : frontières elliptiques

Résumé : Nous proposons une nouvelle classe de conditions aux limites absorbantes de type DtN localisé applicables à des frontières extérieures de forme elliptique lors de la résolution de problèmes de scattering d'ondes acoustiques par des obstacles allongés. Ces conditions sont : (a) exactes pour les premiers modes, (b) faciles à implémenter et à paralléliser, (c) compatibles avec la structure locale d'un schéma numérique de type éléments finis, et (d) applicables à des frontières extérieures de forme elliptique ce qui est plus approprié en terme de coût de calcul lorsque l'on entoure un obstacle allongé. De plus, ces conditions coïncident avec la condition DtN localisée classique construite pour des frontières de forme circulaire. Nous étudions analytiquement et au travers de tests numériques l'effet du régime de fréquence et de l'allongement de la frontière sur la performance de ces conditions lors de la résolution des problèmes de radiateur et de scattering. Nous comparons aussi leurs performances à celles de la condition aux limites absorbante d'ordre deux (BGT2) construite par Bayliss, Gunzburger et Turkel lorsqu'elle est exprimée en coordonnées elliptiques. Cette analyse révèle que, en régime basse fréquence, la condition d'ordre deux DtN (DtN2) admet un très bon niveau de performance *quel que soit* l'allongement de la frontière. De plus, la condition aux limites DtN2 est plus performante que la condition BGT2. Cette supériorité apparaît clairement pour de grandes excentricités.

Mots-clés : Conditions aux limites absorbantes, coordonées elliptiques, opérateur Dirichlet-to-Neumann, problèmes de scattering

1 Introduction

Exterior Helmholtz problems are classical mathematical models for studying scattering problems arising in many applications such as sonar, radar, geophysical exploration, nondestructive testing, etc... Despite their simplicity, this class of problems is not completely solved particularly from a numerical point of view. For example, the computation of the solutions of these problems requires first to limit it to a finite domain. This is often achieved by surrounding the given scatterer(s) (or radiator) by an artificial boundary that is located at some distance (measured in multiples of wavelength of interest) from its surface. A so-called "nonreflecting" boundary condition is then prescribed on the artificial boundary to represent the "far-field" behavior of the scattered field. The challenge here is the development of a simple but reliable as well as cost-effective computational procedure for representing the far-field behavior of the scattered. The quest for such conditions is ongoing (see, e.g., the recent review by Turkel in the book [21]).

We propose in this work new two-dimensional approximate *local* DtN boundary conditions to be employed on elliptical-shaped boundaries that are primary candidates for surrounding elongated scatterers. The idea for constructing such conditions is driven by several considerations chief among them the following two reasons. First, the widely-used second order absorbing boundary condition (BGT2) designed by Bayliss, Gunzburger and Turkel for circular-shaped boundaries [4] performs poorly when it is expressed in elliptical coordinates and applied to elliptical-shaped boundaries in the low frequency regime [16]. The accuracy deteriorates significantly for large eccentricity values of the boundaries as observed in [16]. The damping effect introduced to this condition [17] improves the performance for small eccentricity values. However, the modified BGT2 still performs poorly for eccentricity values larger than 0.6 in the (relatively) low frequency regime (see Figure 6 in [17]). Hence, there is a need for constructing local absorbing boundary conditions (ABC) that extend the range of satisfactory performance. Second, the two-dimensional approximate local DtN conditions designed for circular-shaped boundaries [8] outperforms significantly BGT conditions, particularly for low wavenumber values as reported in [13]. However, using these conditions on circular-shaped exterior boundaries when solving scattering problems by elongated scatterer often leads to larger than needed computational domains, which hampers computational efficiency. This suggests that approximate local DtN boundary conditions designed for elliptical-shaped boundaries is an attractive alternative for improving the computational performance.

Given that, this work is devoted to the construction of theses conditions and to the assessment of their performance when employed for solving two-dimensional acoustic scattering problems by elliptical-shaped obstacles. The idea of constructing two-dimensional approximate *local* DtN boundary conditions is not new. Indeed, as stated earlier, such conditions have been already derived for circular-shaped boundaries [8]. The construction procedure adopted in [8] is based on the localization of the truncated global DtN boundary condition [14]. The key ingredient of this procedure is the trigonometric identities that express high order derivatives of sine and cosine functions (see for example Eq. (A4) p. 276 in [8]). However, this property is not satisfied by the periodic Mathieu functions (see p. 376 in [20]).

Consequently, the procedure used in [8] is no longer applicable to the truncated global DtN boundary operator when expressed in elliptical coordinates [9, 10]. Hence, the construction methodology we propose for deriving the class of approximate local DtN boundary conditions in elliptical coordinates can be viewed as an *inverse-type* approach. More specifically, we start from a Robin-type boundary condition with unknown coefficients. Unlike the case of polar coordinates, these coefficients depend on the angle θ of the elliptical coordinates. Such dependence is necessary to preserve the symmetry and local nature of the resulting boundary conditions. Then, we require that the considered condition to be an exact representation of the first modes. Consequently, the coefficients are the unique solution of a linear algebraic system.

We assess mathematically and numerically the performance of the constructed approximate local DtN boundary conditions. More specifically, we analyze the effect of low wavenumber and the eccentricity on the performance of these conditions in the case of two-dimensional scattering problems. We adopt the on-surface radiation condition formulation (OSRC) [15] in order to perform *analytically* this investigation. We note that such formulation is *not* appropriate for high frequency regime as observed previously in [3]. The main interest in the following analyses is to evaluate the performance of the proposed approximate local DtN conditions at low wavenumber to see if relatively small computational domains can be employed in order to avoid excessive computational cost. The OSRC formulation must be viewed as an extreme case while an exterior elliptical-shaped boundary surrounding an elongated scatterer would be less "demanding" on the boundary condition. The analysis herein shows that the constructed *second-order* local DtN condition retains a good level of accuracy in the low frequency regime for all eccentricity values of the elliptical-shaped boundaries.

2 Preliminaries

Throughout this paper, we use elliptical coordinates (ξ, θ) which are related to the rectangular cartesian ones (x, y) by:

$$x = a\cos\theta \ , \quad y = b\sin\theta \tag{1}$$

where $\theta \in [0, 2\pi)$. The parameters a and b respectively represent the semi-major and semi-minor axes of the ellipse, and are given by:

$$a = f\cosh\xi \ , \quad b = f\sinh\xi \tag{2}$$

where ξ is a strictly positive real number and f is the interfocal distance given by:

$$f = \sqrt{a^2 - b^2} \tag{3}$$

We also define the eccentricity e on the ellipse $\xi = \xi_0$ by:

$$e = \frac{1}{\cosh \xi_0} = \sqrt{1 - \frac{b^2}{a^2}} \tag{4}$$

The eccentricity e characterizes the slenderness of the boundary. It satisfies $0 < e < 1$. Note that when $e \to 0$, the ellipse degenerates into a circle and when $e \to 1$, the ellipse degenerates into a line with length $2f$.
We recall that the n-th elliptic cylindrical mode mode u_n is given by [19] :

$$u_n = \begin{cases} \mathrm{Re}_n^{(3)}(kf, \cosh \xi) Se_n(kf, \cos \theta), & n \geq 0 \,(\text{for } \textit{even} \text{ mode}) \\ \\ \mathrm{Ro}_n^{(3)}(kf, \cosh \xi) So_n(kf, \cos \theta), & n \geq 1 \,(\text{for } \textit{odd} \text{ mode}) \end{cases} \tag{5}$$

where Se_n (resp. So_n) are the *even* (resp. *odd*) *periodic* Mathieu functions, and $\mathrm{Re}_n^{(3)}$ (resp. $\mathrm{Ro}_n^{(3)}$) are the *even* (resp. *odd*) *radial* Mathieu functions of the third kind (see p. 376 in [20]). In addition, the periodic functions Se_n and So_n satisfy the differential equation (see Eq. (15)-(16), p. 377 in Ref. [5]):

$$\frac{\partial^2 v_n}{\partial \theta^2} + \left(c_n - \frac{(kf)^2}{2} \cos^2 \theta \right) v_n = 0 \tag{6}$$

where c_n is called the characteristic value (see p. 376 in Ref. [5] or p. 721 in Ref. [1]). For even modes $v_n = \mathrm{Se}_n$, we have $c_n = a_n := a_n(kf)$, and for odd modes $v_n = \mathrm{So}_n$, we have $c_n = b_n := b_n(kf)$.

3 The new approximate *local* boundary conditions and their derivation

Next, we construct new local DtN absorbing boundary conditions in elliptical coordinates, and describe their properties. Note that, because of the nature of the modes (even and odd), it is possible to construct conditions that are exact representation of the first two even modes or the first two odd modes [18]. We can also construct conditions that are exact, in the least-squares sense, for the first three modes [18]. In the following, we derive and analyze the conditions that are exact representation of the even modes. The construction of the other conditions can be found in [18]. We must point out that the performance of all these conditions is comparable as demonstrated in [18].

3.1 The approximate local DtN boundary conditions in elliptical coordinates

The two-dimensional first- (DtN1) and second-order (DtN2) local Dirichlet-to-Neumann boundary conditions, defined on the elliptical-shaped surface $\xi = \xi_0$, are given by:

$$\text{DtN1}: \quad \frac{\partial\, u}{\partial \xi} = \frac{\sqrt{1-e^2}}{e}\, r_0\, u \tag{7}$$

$$\text{DtN2}: \quad \frac{\partial u}{\partial \xi} = \frac{\sqrt{1-e^2}}{(a_0-a_1)e}\left[\left(a_0 r_1 - a_1 r_0 - (r_0-r_1)\,\frac{(eka)^2}{2}\cos 2\theta\right) u + (r_1-r_0)\frac{\partial^2 u}{\partial \theta^2}\right] \tag{8}$$

where the coefficients r_n depend on the *even* radial Mathieu functions of the third kind $\mathrm{Re}_n^{(3)}$, the wavenumber ka, and the eccentricity e as follows:

$$r_n = \frac{\dfrac{\partial \mathrm{Re}_n^{(3)}}{\partial \xi}(eka, e^{-1})}{\mathrm{Re}_n^{(3)}(eka, e^{-1})} \;; \quad n \geq 0 \tag{9}$$

The following four remarks are noteworthy:

- First, the Robin-type boundary conditions (7)-(8) are, by construction, an exact representation of the first elliptical mode u_0 given by Eq. (5). The boundary condition (8) is an exact of the second *even* mode u_1 (see Eq. (5)). On can find in Ref. [18] the construction of a second-order DtN boundary condition that is exact for the first mode u_0 and the second *odd* mode u_1, as well as a second-order DtN boundary conditions that is exact, in the least-squares sense, for the first mode u_0, the second *even* mode u_1, and the second *odd* mode u_1. The performance of all these second-order DtN conditions are comparable if not identical as demonstrated in [18].

- Second, the boundary conditions (7), (8) are called *local* DtN conditions because they result from a localization process of the truncated global DtN boundary operator defined in [9, 10]. The local feature of these conditions is of a great interest from a numerical view point. Indeed, the incorporation of these conditions in any finite element code introduces only mass- and stiffness-type matrices defined on the exterior boundary. The coefficients a_n and r_n can be computed once for all at the preprocessing level.

- Third, it must be point out that when $e = 0$ (the ellipse becomes a circle), conditions (7) and (8) are identical to the two-dimensional DtN conditions designed for circular shaped boundaries [12, 13]. This property can be easily established using the asymptotic behavior of the *even* radial Mathieu functions of the third kind $\mathrm{Re}_n^{(3)}$ and the *even* characteristic values a_n.

- Last, approximate local DtN boundary conditions of order higher than two are inappropriate for conventional finite element implementations since they require regularity higher than C^0. Consequently, we consider only the first (DtN1) and second order (DtN2) conditions in the following.

3.2 The procedure for constructing the approximate local DtN conditions

As stated earlier in the introduction, the idea of constructing approximate *local* DtN boundary conditions is not new. Indeed, such conditions have been already derived for spherical-shaped boundaries in [12]. The construction procedure adopted in [12] is based on the localization of the truncated global DtN boundary condition [10]. The key ingredient of this procedure is the trigonometric identities that express high order derivatives of sine and cosine functions (see for example Eq. (A4) p. 276 in [8]). However, this property is not satisfied by the angular Mathieu functions (see Eq. (6)), and therefore, the procedure used in [12] cannot be applied to the truncated global DtN boundary operator when expressed in elliptical coordinates [9, 10]. The approach we propose for constructing these approximate local DtN boundary condition in the case of elliptical-shaped boundaries can be viewed as an *inverse-type* methodology. More specifically, we start from a Robin-type boundary condition with unknown coefficients. These coefficients depend on the elliptical characteristic values. In addition, we require that the considered condition is an exact representation of the first modes. Consequently, the coefficients are the unique solution of a linear algebraic system. Next, we describe this procedure for construction the approximate local DtN1 and DtN2 conditions given by Eqs. (7)–(8).

i. *Construction of the first order DtN1 boundary condition*

We consider a Robin-type boundary condition that is an exact representation of the first elliptical mode u_0 given by Eq. (5). Hence, we set:

$$\frac{\partial u}{\partial \xi} = Au \tag{10}$$

where the constant A satisfies

$$\sinh\xi \, \frac{\partial \mathrm{Re}_0^{(3)}}{\partial \xi}(kf, \cosh\xi)\, Se_0(kf, \cos\theta) = A \left(\mathrm{Re}_0^{(3)}(kf, \cosh\xi)\, Se_0(kf, \cos\theta) \right) \tag{11}$$

Then, we substitute, at $\xi = \xi_0$, Eqs. (2), (3), (4) into Eq. (11), and deduce that:

$$A = \frac{\sqrt{1-e^2}}{e} r_0 \tag{12}$$

where r_0 is given by Eq. (9) for $n = 0$.

ii. *Construction of the even second order DtN2 boundary condition*

The goal here is to construct a Robin-type boundary condition that is an exact representation of the first two modes u_0 and $u_{1,\mathrm{even}}$ given by Eq. (5). Hence, we set:

$$\frac{\partial u}{\partial \xi} = C\, u + D \left(\frac{\partial^2}{\partial \theta^2} - \frac{(eka)^2}{2} \cos 2\theta \right) u \tag{13}$$

where C and D are constant (independent of θ) to be determined. Note that, unlike DtN2 boundary condition for the circular-shaped boundaries, the coefficients of this condition depend on the angular variable θ. Such dependence is necessary for constructing a *symmetric* boundary condition since the angular Mathieu functions satisfied differential equation given by Eq. (6). Indeed, it is easy to verify that, for all *even* modes u_n, we have:

$$\frac{\partial^2 u_n}{\partial \theta^2} = \left(-a_n + \frac{(eka)^2}{2} \cos 2\theta \right) u_n \tag{14}$$

In order to determine the constants C and D, we assume that, at $\xi = \xi_0$, we have:

$$\frac{\partial u_n}{\partial \xi} = C\, u_n + D \left(\frac{\partial^2}{\partial \theta^2} - (\frac{(eka)^2}{2} \cos 2\theta \right) u_n \; ; \quad n = 0 \quad \text{and} \quad n = 1 (even \text{ mode}) \tag{15}$$

Then, using Eq. (14), it follows that (C, D) is the unique solution of the folllowing 2×2 linear system:

$$\begin{cases} C - D\, a_0 = \dfrac{\sqrt{1-e^2}}{e}\, r_0 \\ \\ C - D\, a_1 = \dfrac{\sqrt{1-e^2}}{e}\, r_1 \end{cases} \tag{16}$$

where the coefficients r_n are given by Eq. (9).
The DtN2 even boundary condition given by Eq. (8) is a direct consequence of solving the system (16) and then substituting the expressions of (C, D) into Eq. (13).

4 The performance of the new approximate local DtN conditions

In the following, we assess analytically and numerically the performance of the approximate local DtN1 and DtN2e boundary conditions given by (7) and (8). More specifically, we analyze the effect of low wavenumber ka and the eccentricity e on the performance of DtN1 and DtN2e in the case of both radiator and scattering problems. We adopt the on-surface radiation condition formulation (OSRC) [15] in order to perform this investigation analytically. We note that such formulation is not appropriate for high frequency regime as observed previously in [3]. The main interest in the following analyses is to evaluate the performance of the proposed approximate local DtN conditions at low ka to see if relatively small computational domains can be employed in order to avoid excessive computational cost. The OSRC formulation is an extreme case while an exterior elliptical-shaped artificial boundary surrounding an elongated scatterer would be less "demanding" on the boundary

condition. As in [13, 16, 17], we assess the performance of the ABCs DtN1 and DtN2 using the *specific impedance* introduced in [6, 7] as a practical tool for measuring the efficiency of ABCs in the context of the OSRC formulation. This *non-dimensional* quantity measures the effect of the truncated medium in physical terms. It provides a convenient indicator of the performance of a given approximate representation. In the elliptical coordinates system, the specific impedance can be expressed as follows:

$$Z = \frac{i\sqrt{1-e^2}\,ka\,u}{\dfrac{\partial u}{\partial \xi}}\,|_{\xi=\xi_0} \tag{17}$$

4.1 The performance of the local DtN conditions for single elliptical mode

Next, we assess analytically and numerically the performance of the approximate local DtN1 and DtN2 boundary conditions given by (7) and (8) when applied to two-dimensional radiator problems. Recall that the exact specific impedance Z_n^{ex2}, for the nth *even* mode, on the boundary of an ellipse at $\xi = \xi_0$ is given by (see Eq. (13), p. 3626 in [16]):

$$Z_n^{\mathrm{ex2}} \;=\; \frac{\mathrm{i}\,eka\,\mathrm{Re}_n^{(3)}(eka, e^{-1})}{\dfrac{\partial \mathrm{Re}_n^{(3)}}{\partial \xi}(eka, e^{-1})} \;=\; \frac{\mathrm{i}\,eka}{r_n} \tag{18}$$

where the coefficient r_n is given by Eq. (9). In addition, its asymptotic behavior as $ka \to 0$ (see Eq. (17), p. 3627 in [16]) is given by:

$$Z_n^{\mathrm{ex2}} \sim \begin{cases} \pi\dfrac{ka}{2} + \mathrm{i}\,ka\ln(ka) & \text{if } n = 0 \\[2ex] \dfrac{4\pi}{(n!)^2}\left(\dfrac{ka}{2}\right)^{(2n+1)} - \mathrm{i}\,\dfrac{ka}{n} & \text{if } n \geq 1 \end{cases} \tag{19}$$

4.1.1 Analytical study

The following lemma states the expression of the approximate specific impedances for the n-th even elliptical mode, on the surface of an ellipse at $\xi = \xi_0$. This lemma results from substituting $u = u_n$ in Eq. (17), and using the boundary conditions (7) and (8) to evaluate $\dfrac{\partial u_n}{\partial \xi}$ (see [18] for the detailed proof).

Lemma 4.1 *The approximate specific impedance (Z_n^{DtN1}) corresponding to the first-order Dirichlet-to-Neumann boundary condition (DtN1) is given by:*

$$Z_n^{\mathrm{DtN1}} = Z_0^{\mathrm{ex2}} \tag{20}$$

The approximate specific impedance (Z_n^{DtN2e}) corresponding to the second-order Dirichlet-to-Neumann boundary condition (DtN2e) is given by:

$$Z_n^{\mathrm{DtN2}} = \frac{1}{\dfrac{1}{Z_0^{\mathrm{ex2}}} + \dfrac{a_0 - a_n}{a_0 - a_1}\left[\dfrac{1}{Z_1^{\mathrm{ex2}}} - \dfrac{1}{Z_0^{\mathrm{ex2}}}\right]} \tag{21}$$

where $a_n := a_n(kf)$ is the characteristic value corresponding to the nth even periodic Mathieu function Se_n (see p. 376 in Ref. [5] or p. 721 in Ref. [1]).

Remark 4.2 Note that when $e \to 0$, that is the ellipse degenerates to a circle, the approximate DtN specific impedances given by Eqs. (20) and (21) are identical to the ones obtained in the case of circular-shaped radiators [13]. In addition, when $n = 0$ (resp. $n = 1$ for *even* mode), Z_n^{DtN2} coincides with Z_0^{ex2} (resp. with Z_1^{ex2}), as expected.

The next proposition states the asymptotic behavior of the approximate specific impedance Z_n^{DtN2} as $ka \to 0$.

Proposition 4.3 *The asymptotic behavior of the DtN2e specific impedance of the nth elliptical even mode as $ka \to 0$ is given by:*

$$Z_n^{\mathrm{DtN2}} \sim \frac{\pi}{2n^2}(ka)^3 - \mathrm{i}\frac{ka}{n^2}; \quad n \geq 2 \tag{22}$$

Proof of Proposition 4.3. First, observe that (see Eq. (36) p. 120 in Ref. [**?**]):

$$a_0 \sim -\frac{(eka)^4}{32} \text{ when } ka \to 0 \tag{23}$$

$$a_n(0) = n^2 \text{ for } n \geq 1 \tag{24}$$

Therefore, when $ka \to 0$, it follows from that the approximate DtN2 specific impedance given by Eq. (21) is equivalent to the following function:

$$\phi(ka) = \frac{1}{\dfrac{1}{\pi\dfrac{ka}{2} + \mathrm{i}ka\ln(ka)} + \dfrac{-\dfrac{(eka)^4}{32} - n^2}{-\dfrac{(eka)^4}{32} - 1}\left[\dfrac{1}{\dfrac{\pi}{2}(ka)^3 - \mathrm{i}ka} - \dfrac{1}{\pi\dfrac{ka}{2} + \mathrm{i}ka\ln(ka)}\right]}; \quad n \geq 2 \tag{25}$$

and the result of Proposition 4.3 follows from a suitable truncation of a Taylor expansion when ka tends to 0.

Remark 4.4 First, we note that the asymptotic behavior of Z_n^{DtN1} (resp. Z_n^{DtN2} ; $n \leq 1$) is identical to the behavior of the exact specific impedance Z_0^{ex2} (resp. Z_n^{ex2} ; $n \leq 1$), which follows from the design of the DtN boundary conditions. Second, for $n \geq 2$, the asymptotic behavior for DtN2 is independent of the eccentricity e, and is identical to the case of a circle

(see Eq.(62), p. 27 in [13]) as well as to the approximate specific impedance corresponding to the second-order BGT condition when applied on elliptical radiator (see Eq. (19), p. 3627 in [16]). Last, the asymptotic behavior given by Eq. (19) and Eq. (22) indicates that for higher modes ($n \geq 2$), the real part of the exact impedance tends to zero, as $ka \to 0$, faster than the DtN2 specific impedance. This result suggests that DtN2 boundary condition may not be appropriate for single higher modes.

4.1.2 Numerical investigation

We have performed several experiments to investigate numerically the effect of the wavenumber and the slenderness of the boundary on the performance of the second-order DtN boundary condition DtN2 given by Eq. (8) when computing single radiating modes. We have compared the results to the ones obtained with BGT2 conditions when applied on elliptical-shaped boundaries (see Figs. (2) to (8) in [16]). We report in here the results obtained for three different even modes $n = 1$, $n = 2$, $n = 3$ for illustration (see Figs. (1)–(5)). More numerical results can be found in [18]. These results have been obtained for three eccentricity values $e = 0.1$ corresponding to an elliptical-shaped boundary very close to a circle, $e = 0.6$ corresponding to a "regular" elliptical boundary, and $e = 0.9$ corresponding to a very elongated elliptical boundary. Because of the dependence of the BGT2 specific impedance on $\theta \in [0, 2\pi)$ (see Eq. (15) in [16]), we have reported the obtained results on the magnitude of the specific impedance in polar coordinates, and the relative errors as a function of θ (see Figs. (2)–(5)).

Fig. 1 illustrates the performance of the first-order condition DtN1 versus the BGT1 condition when computing the second even elliptical mode u_1. One can observe that both conditions perform overall very poorly. When $ka = 1$ as indicated by the magnitude of the relative error in the right of Fig. 1. Figs. (2)–(5) compare the performance of the approximate second-order DtN2 and BGT2 boundary conditions when computing higher order *even* modes (u_2, u_3) for two low wavenumber values $ka = 0.1$ and $ka = 1$. The results indicate that both conditions perform poorly and therefore are not appropriate for computing higher modes. Note that the second-order DtN2 boundary outperform the BGT2 boundary condition when computing the first two modes u_0 and u_1 (*even*) since the DtN2 condition is an exact representation of these two modes.

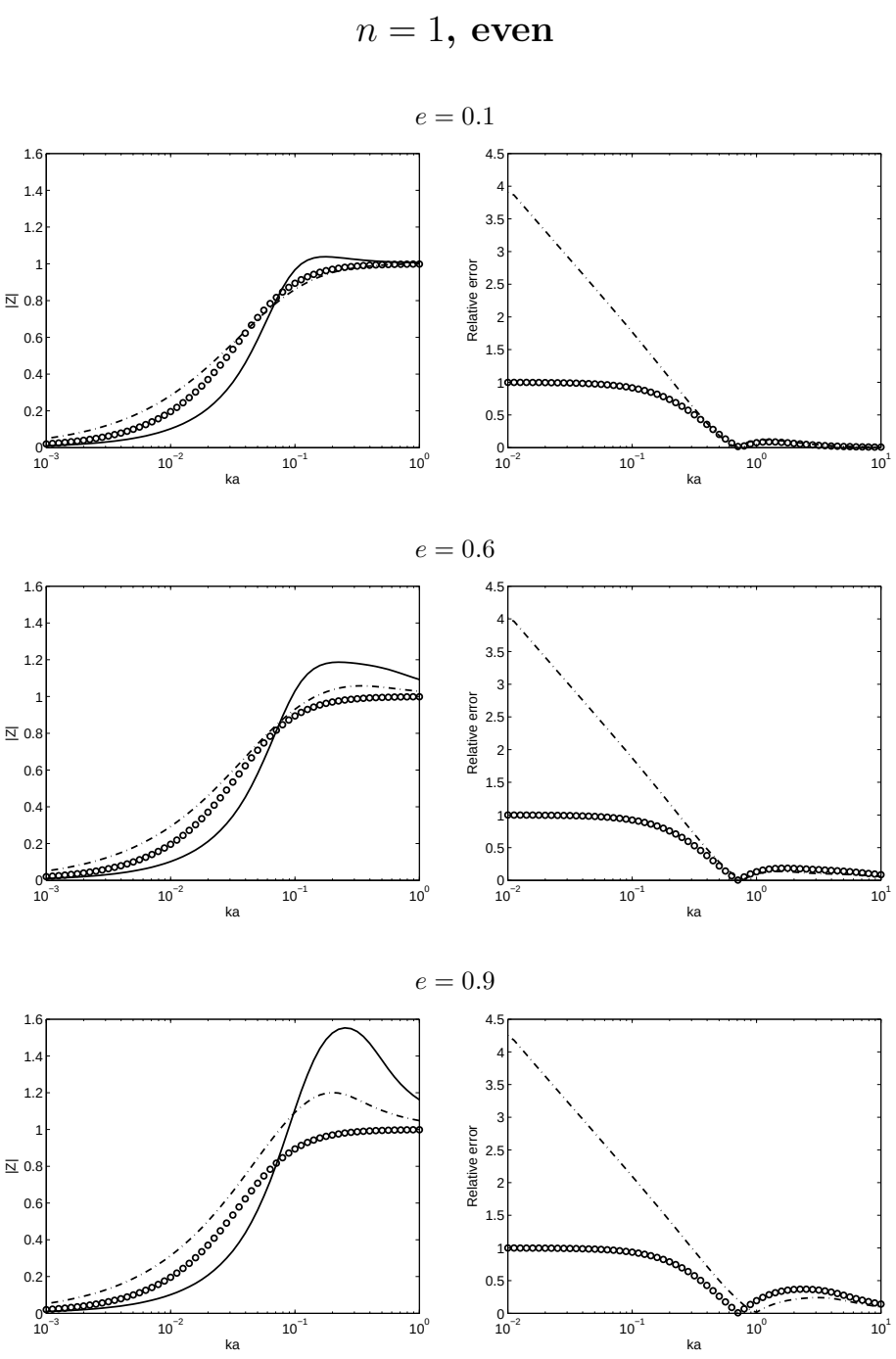

Figure 1: Absolute value (left) and relative error (right) of the specific impedance for the exact (solid), the DtN1 (dash), the BGT1 (circle).

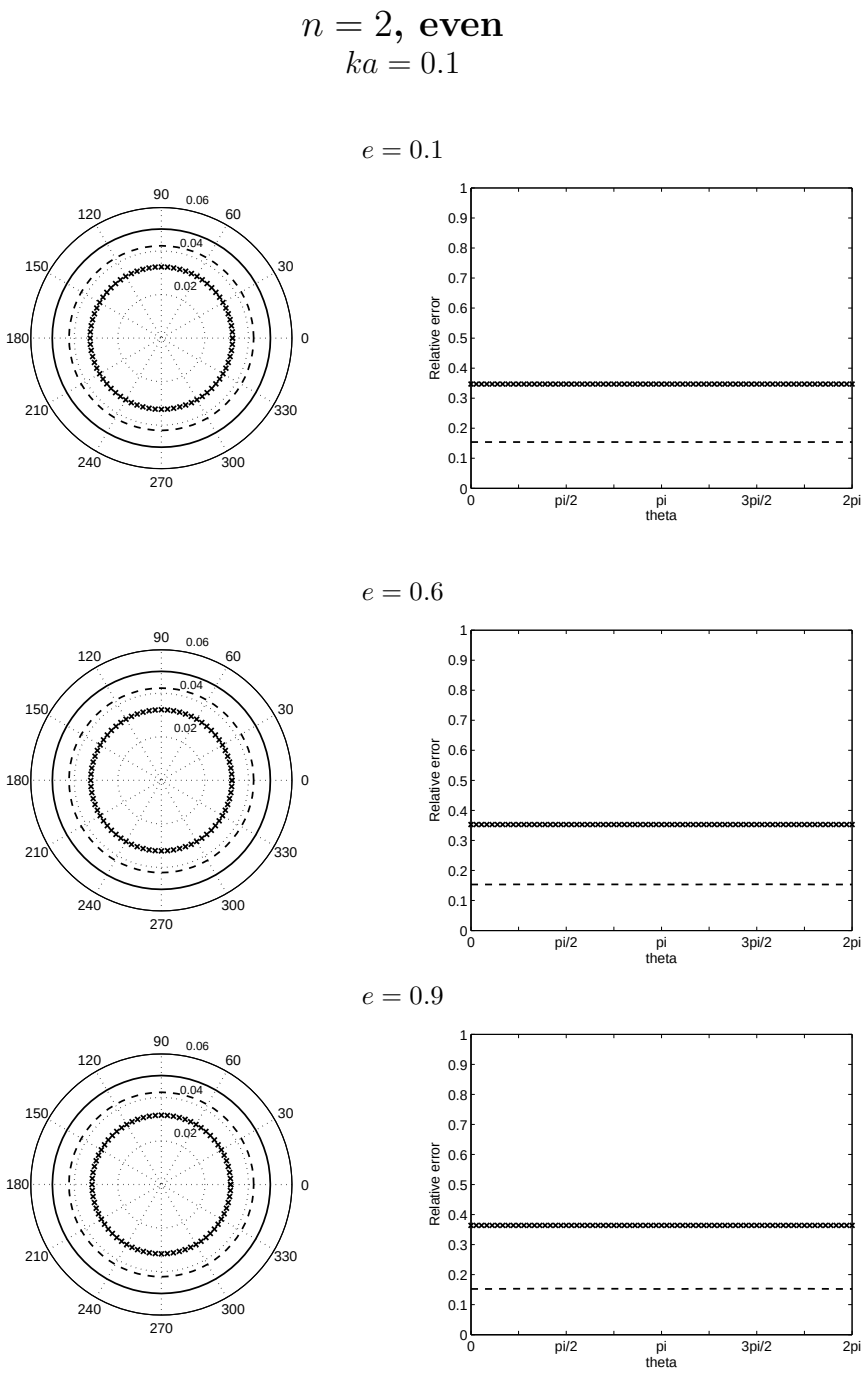

Figure 2: Absolute value (left) and relative error (right) of the specific impedance for the exact (solid), the DtN2 (crossed), the BGT2 (dashed).

$n = 2$, **even**
$ka = 1$

$e = 0.1$

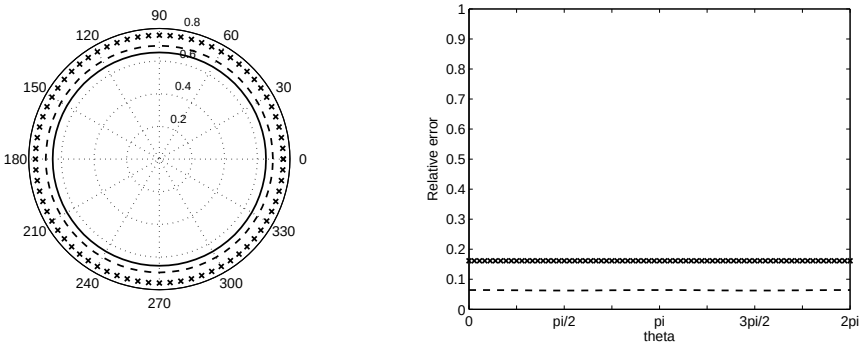

$e = 0.6$

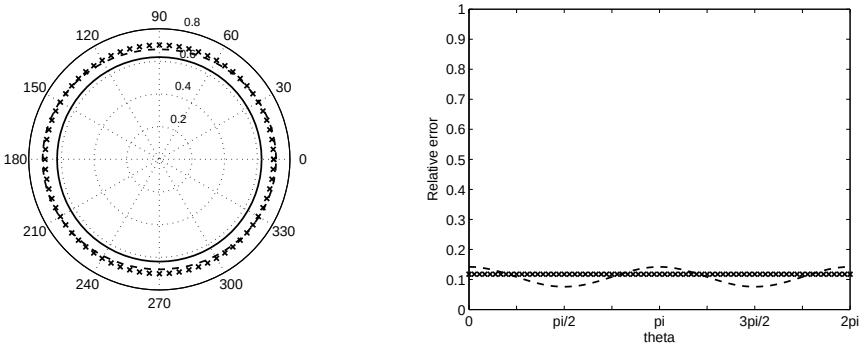

$e = 0.9$

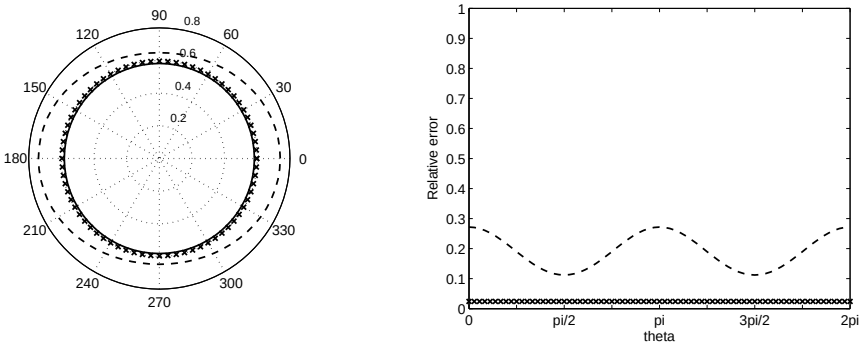

Figure 3: Absolute value (left) and relative error (right) of the specific impedance for the exact (solid), the DtN2 (crossed), the BGT2 (dashed).

$n = 3$, **even**
$ka = 0.1$

$e = 0.1$

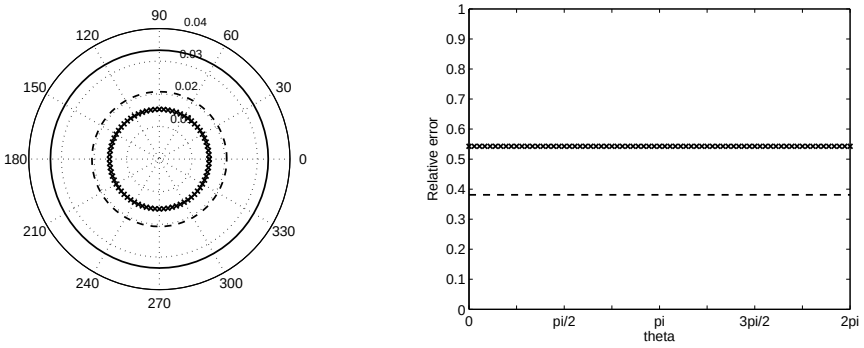

$e = 0.6$

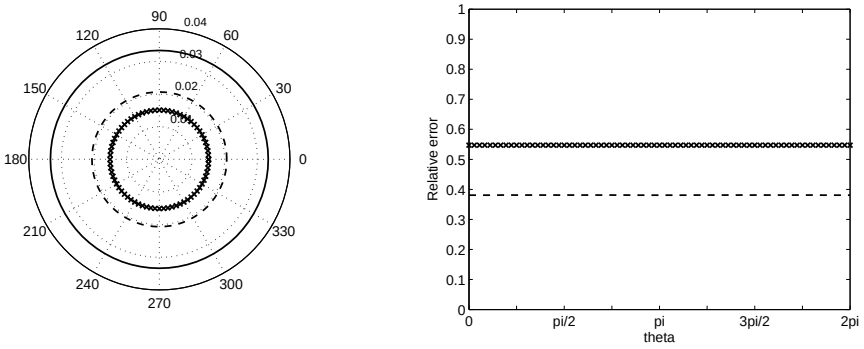

$e = 0.9$

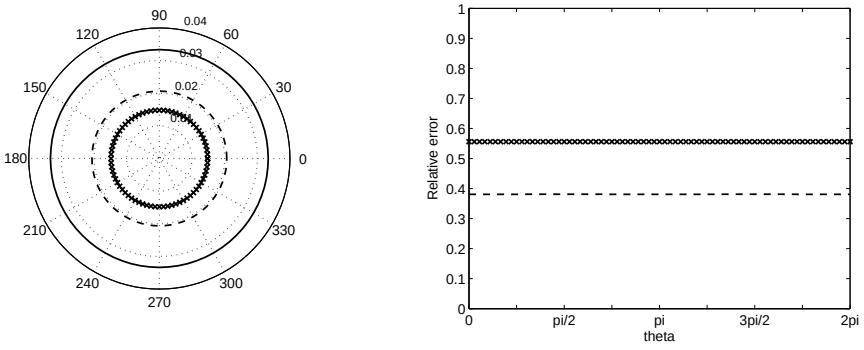

Figure 4: Absolute value (left) and relative error (right) of the specific impedance for the exact (solid), the DtN2 (crossed), the BGT2 (dashed).

$n = 3$, **even**
$ka = 1$

$e = 0.1$

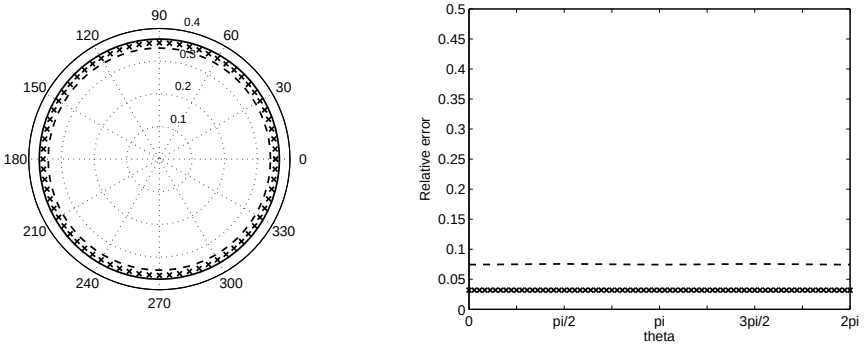

$e = 0.6$

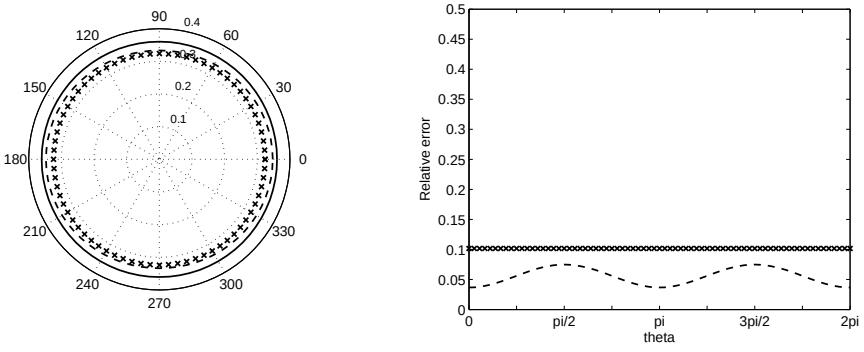

$e = 0.9$

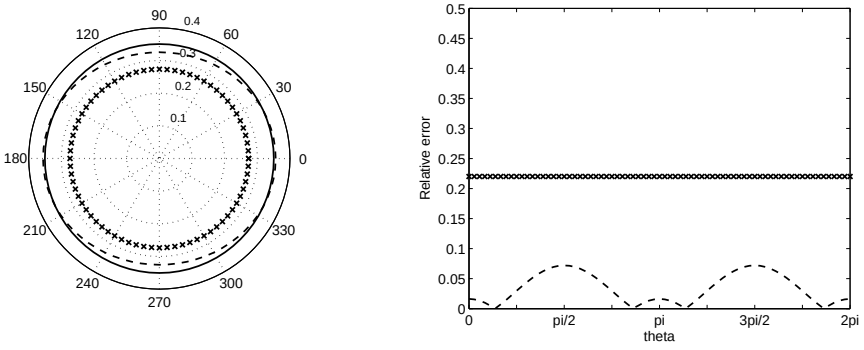

Figure 5: Absolute value (left) and relative error (right) of the specific impedance for the exact (solid), the DtN2 (crossed), the BGT2 (dashed).

4.2 The performance of the local DtN conditions for elliptical-shaped scatterer

Next, we assess analytically and numerically the performance of the approximate local DtN1 and DtN2 boundary conditions given by (7) and (8) when applied to two-dimensional scattering problems by sound-soft elliptical-shaped obstacle. Recall (see Eq. (33), p. 3635 in Ref. [16]), that the exact specific impedance Z^{ex2} on the surface of an ellipse at $\xi = \xi_0$ is given by:

$$Z^{\text{ex2}} = -\frac{\mathrm{i}\sqrt{1-e^2}ka\, u^{\text{inc}}}{\dfrac{\partial}{\partial\xi}\,(u^{\text{scat}})|_{\xi=\xi_0}} \tag{26}$$

where u^{inc} is the incident plane wave with incident angle θ_0 defined by:

$$u^{\text{inc}} = \mathrm{e}^{\mathrm{i}kf\cosh\xi(\cos\theta\cos\theta_0+\tanh\xi\sin\theta\sin\theta_0)} \tag{27}$$

and u^{scat} is the acoustic scattered field by a sound-soft elliptical-shaped obstacle. u^{scat} can be represented by the following series [**?**]:

$$u^{\text{scat}} = -\sqrt{8\pi}\left(\sum_{m=0}^{\infty}\mathrm{i}^m Ke_m Re_m^{(3)}(kf,\cosh\xi)Se_m(kf,\cos\theta) + \sum_{m=1}^{\infty}\mathrm{i}^m Ko_m Ro_m^{(3)}(kf,\cosh\xi)So_m(kf,\cos\theta)\right) \tag{28}$$

where

$$\begin{aligned} Ke_m &= \frac{1}{N_m^{(e)}}\frac{\mathrm{Re}_m^{(1)}(eka,e^{-1})\mathrm{Se}_m(eka,\cos\theta_0)}{\mathrm{Re}_m^{(3)}(eka,e^{-1})} \\ Ko_m &= \frac{1}{N_m^{(o)}}\frac{\mathrm{Ro}_m^{(1)}(eka,e^{-1})\mathrm{Se}_m(eka,\cos\theta_0)}{\mathrm{Ro}_m^{(3)}(eka,e^{-1})} \end{aligned} \tag{29}$$

and $N_m^{(e)}$ (resp. $N_m^{(o)}$) represents the normalization factor of the even (resp. odd) angular Mathieu functions (see Eq. (18), p. 377 in Ref. [20]).
Moreover, we also recall (see Eq.(38), p. 3637 in [16]), that the asymptotic behavior of the exact specific impedance Z^{ex2} of the scattered field on the surface of an ellipse as ka approaches 0 is given by:

$$Z^{\text{ex2}} \sim Z_0^{\text{ex2}} \sim \pi\frac{ka}{2} + \mathrm{i}ka\ln(ka)\ ; \quad ka \to 0 \tag{30}$$

where Z_0^{ex2} is given by Eq. (19).

4.2.1 Analytical study

The next lemma states the expression of the approximate specific impedances on the boundary $\xi = \xi_0$ of an elliptical-shaped sound-soft scatterer. This lemma results from substituting

$u = -u^{\text{inc}}$ in Eq. (17), and using the boundary conditions (7) and (8), and the expression of the incident plane wave given by Eq. (27) to evaluate $\dfrac{\partial u^{\text{inc}}}{\partial \xi}$ at $\xi = \xi_0$ (see [18] for the detailed proof).

Lemma 4.5 *The approximate specific impedance ($Z^{\text{DtN1,2D}}$) corresponding to the first-order Dirichlet-to-Neumann boundary condition (DtN1) is given by:*

$$Z^{\text{DtN1}} = Z_0^{\text{ex2}} \tag{31}$$

The approximate specific impedance (Z^{DtN2}) corresponding to the even second-order Dirichlet-to-Neumann boundary condition (DtN2) is given by:

$$Z^{\text{DtN2}} = \frac{1}{\dfrac{1}{Z_0^{\text{ex2}}} + \dfrac{1}{a_0 - a_1}\left(\delta + a_0\right)\left(\dfrac{1}{Z_1^{\text{ex2}}} - \dfrac{1}{Z_0^{\text{ex2}}}\right)} \tag{32}$$

where

$$\begin{aligned} \lambda &= \cos\theta\cos\theta_0 + \sqrt{1-e^2}\sin\theta\sin\theta_0 \\ \delta &= -ika\lambda - (ka)^2\left(\frac{\partial\lambda}{\partial\theta^2}\right) - \frac{(eka)^2}{2}\cos 2\theta \end{aligned} \tag{33}$$

Remark 4.6 Note that when $e \to = 0$, that is the ellipse degenerates to a circle, the approximate DtN specific impedances given by Eqs. (31) and (32) are identical to the ones obtained in the case of circular-shaped scatterers [13].

The next proposition states the asymptotic behavior of the second-order DtN approximate specific impedance Z^{DtN2} as $ka \to 0$.

Proposition 4.7 *The asymptotic behavior of the approximate specific impedance $Z^{\text{DtN2e,2D}}$ as $ka \to 0$ is given by:*

$$Z^{\text{DtN2e,2D}} \sim Z_0^{\text{ex2}} \tag{34}$$

Proof of Proposition 4.7. According to (34), we have:

$$Z^{\text{DtN2e,2D}} = Z_0^{\text{ex2}} \frac{1}{1 + \dfrac{a_0 + \delta}{a_0 - a_1}\left[\dfrac{Z_0^{\text{ex2}}}{Z_{1,even}^{\text{ex2}}} - 1\right]} \tag{35}$$

Next, from the definition of δ, we can write that:

$$\delta = -ika\Psi_1(ka) \quad \text{with } \Psi_1(ka) \to \lambda \text{ when } ka \to 0 \tag{36}$$

which implies, using (23), that:

$$a_0 + \delta = -ika\Psi_2(ka) \quad \text{with } \Psi_2(ka) \to \lambda \text{ when } ka \to 0 \tag{37}$$

Next, (24) and (23) imply that:

$$a_1 - a_0 \to 1 \quad \text{when } ka \to 0 \tag{38}$$

We then use (32) to obtain that when $ka \to 0$, $\dfrac{Z_0^{\text{ex2}}}{Z_{1,even}^{\text{ex2}}} - 1$ behaves like $\Psi_3(ka)$ with:

$$\Psi_3(ka) = \ln(ka) + i\frac{\pi}{2} \tag{39}$$

Hence, from (37), (38) and (39) we deduce that:

$$\frac{a_0 + \delta}{a_0 - a_1}\left[\frac{Z_0^{\text{ex2}}}{Z_{1,even}^{\text{ex2}}} - 1\right] \to 0 \quad \text{when } ka \to 0 \tag{40}$$

and we conclude that:

$$Z^{\text{DtN2e,2D}} \sim Z_0^{\text{ex2}} \tag{41}$$

Remark 4.8 First, we note that, unlike the approximate specific impedance coresponding to the secon-order BGT2 condition, the asymptotic behavior, as $ka \to 0$, of Z^{DtN2} is identical to the behavior of the exact specific impedance Z^{ex2} (see Eq. (30). In addition, when $e = 0$, the asymptotic of both Z^{DtN1} and Z^{DtN2} are identical to the case of circular-shaped sound-soft scatterers.

4.2.2 Numerical investigation

We have performed several experiments to investigate numerically the effect of the wavenumber and the slenderness of the boundary on the performance of the second-order DtN boundary condition DtN2 given by Eq. (8) when solving sound-soft scattering problems in the OSRC context. We have compared the results to the ones obtained with BGT2 conditions when applied on elliptical-shaped boundaries boundaries (see Figs. (9) to (13) in [16]). We report in here the results obtained for three different values of the incidence angle $\theta_0 = 0, \dfrac{\pi}{4}$, and $\dfrac{\pi}{2}$ for illustration. More numerical results can be found in [18]. Moreover, since the impedances in this case depend on the observation angle $\theta \in [0, 2\pi)$, we have reported in Figs (6)–(8) in polar coordinates the magnitude of the impedances. In addition, we have reported in Figs. (9)–(11) the relative errors as a function the observation angle θ. These results have been obtained for three eccentricity values $e = 0.1$ corresponding to a elliptical-shaped boundary very close to a circle (see Fig. (6) and Fig. (9)), $e = 0.6$ corresponding to a "regular" ellipse (see Fig. (7) and Fig. (10)), and $e = 0.9$ corresponding to a very elongated ellipse (see Fig. (8) and Fig. (11)). These results indicate that

i. Unlike the radiator problem, the second-order DtN2 absorbing boundary condition retains an excellent level of accuracy when solving acoustic problems for low number,

as expected (see Proposition 4.7). In addition, the results reported in Figs. (9)–(11), clearly indicate that the good performance of DtN2 boundary condition is not sensitive to values of the eccentricity e. These results suggest that the second-order DtN absorbing boundary condition given by Eq. (8) is appropriate for elongated boundaries.

ii. The second-order DtN2 absorbing boundary condition clearly outperforms the second-order BGT2 absorbing boundary condition especially for high eccentricity values. Indeed, there is a significant loss of accuracy for BGt2 boundary condition when $e \geq 0.6$ (see Figs. (10)–(11)). This demonstrates that the second-order DtN2 boundary condition extends the range of satisfactory performance to all eccentricity values.

iii. For some particular observation angles, the first-order DtN1 boundary condition performs surprisingly better than the second-order DtN2 boundary condition (see Figs. (9)–(11)). Nevertheless, the *total* relative error (the average of the relative error over all observation angles) delivered by DtN1 boundary condition is significantly higher than the *total* relative error corresponding to the second-order DtN2 boundary condition.

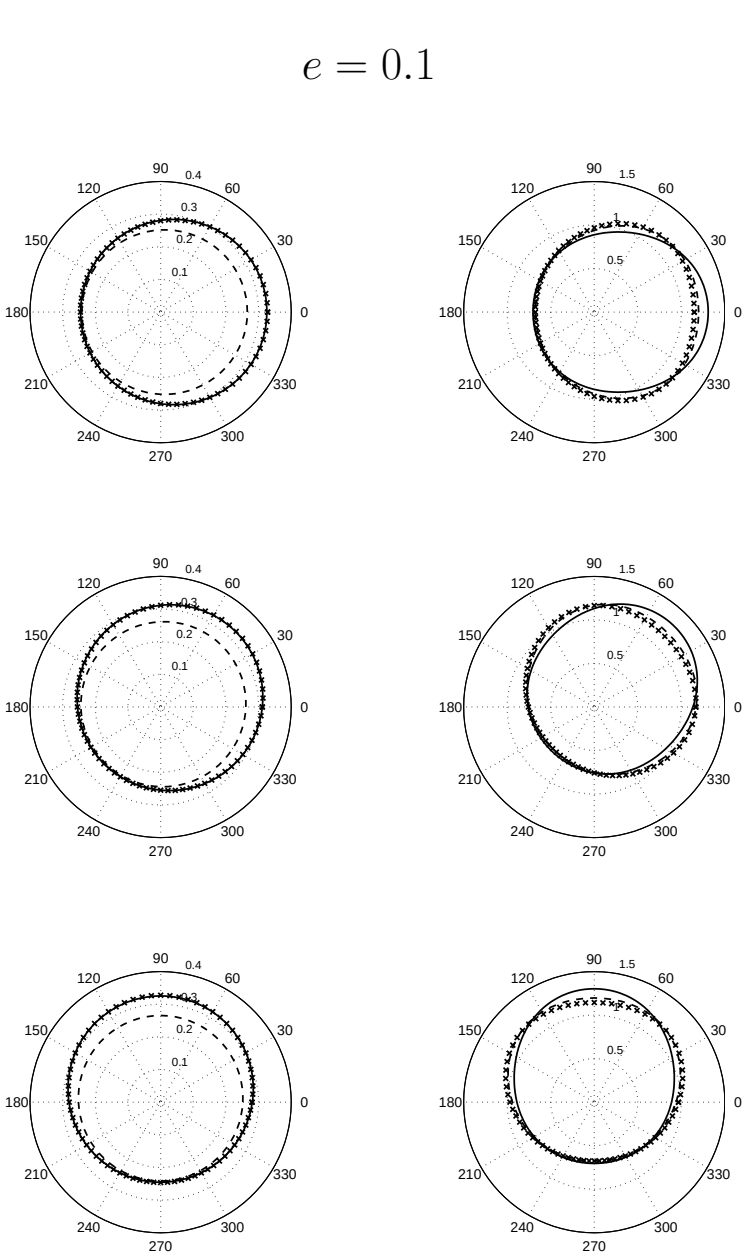

Figure 6: Absolute value of the specific impedance for the exact (solid), the DtN2 (crossed), the BGT2 (dashed) for $ka = 0.1$ (left) and $ka = 1$ (right) for the incident angles $\theta_0 = 0$ (up), $\theta_0 = \frac{\pi}{4}$ (middle), $\theta_0 = \frac{\pi}{2}$ (down).

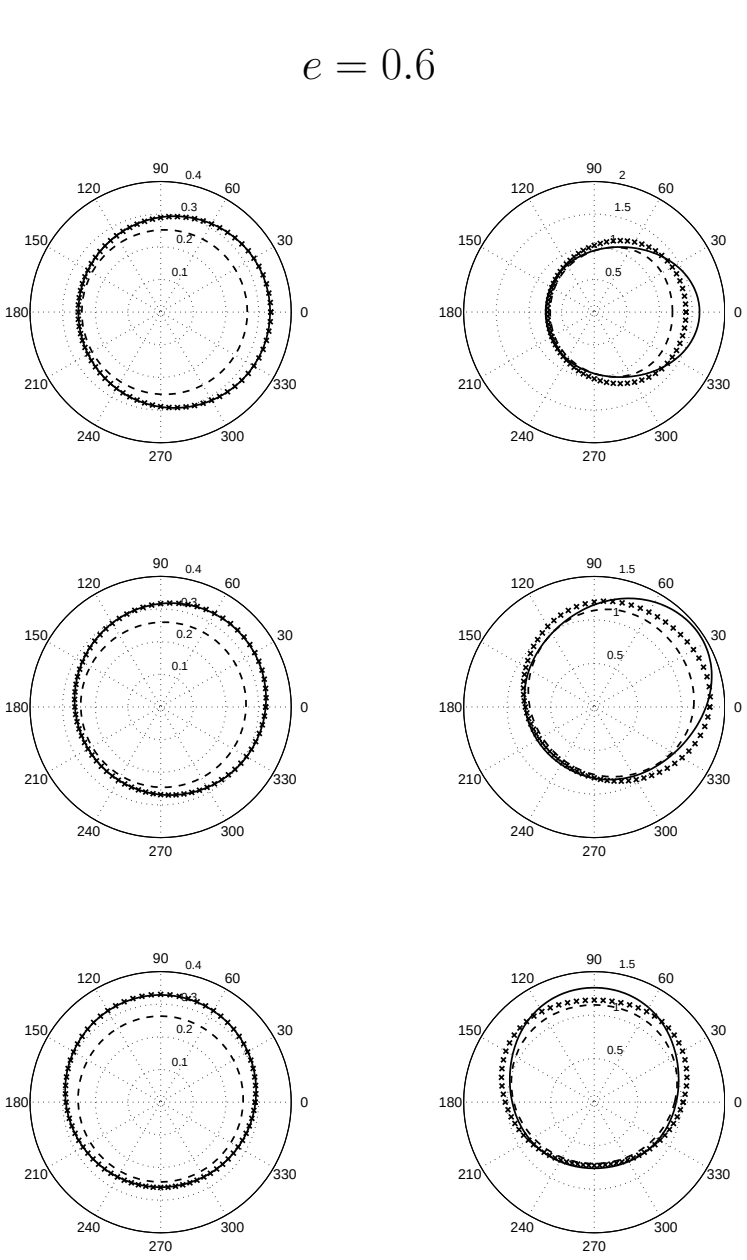

Figure 7: Absolute value of the specific impedance for the exact (solid), the DtN2 (crossed), the BGT2 (dashed) for $ka = 0.1$ (left) and $ka = 1$ (right) for the incident angles $\theta_0 = 0$ (up), $\theta_0 = \frac{\pi}{4}$ (middle), $\theta_0 = \frac{\pi}{2}$ (down).

$e = 0.9$

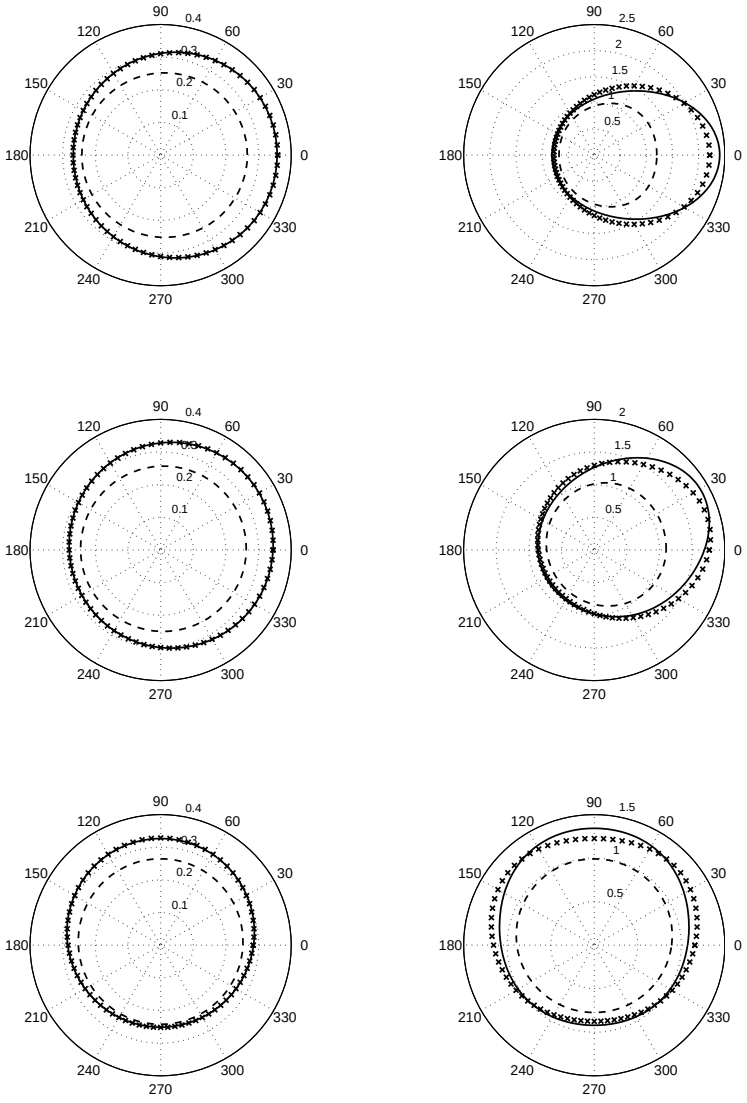

Figure 8: Absolute value of the specific impedance for the exact (solid), the DtN2 (crossed), the BGT2 (dashed) for $ka = 0.1$ (left) and $ka = 1$ (right) for the incident angles $\theta_0 = 0$ (up), $\theta_0 = \frac{\pi}{4}$ (middle), $\theta_0 = \frac{\pi}{2}$ (down).

$e = 0.1$

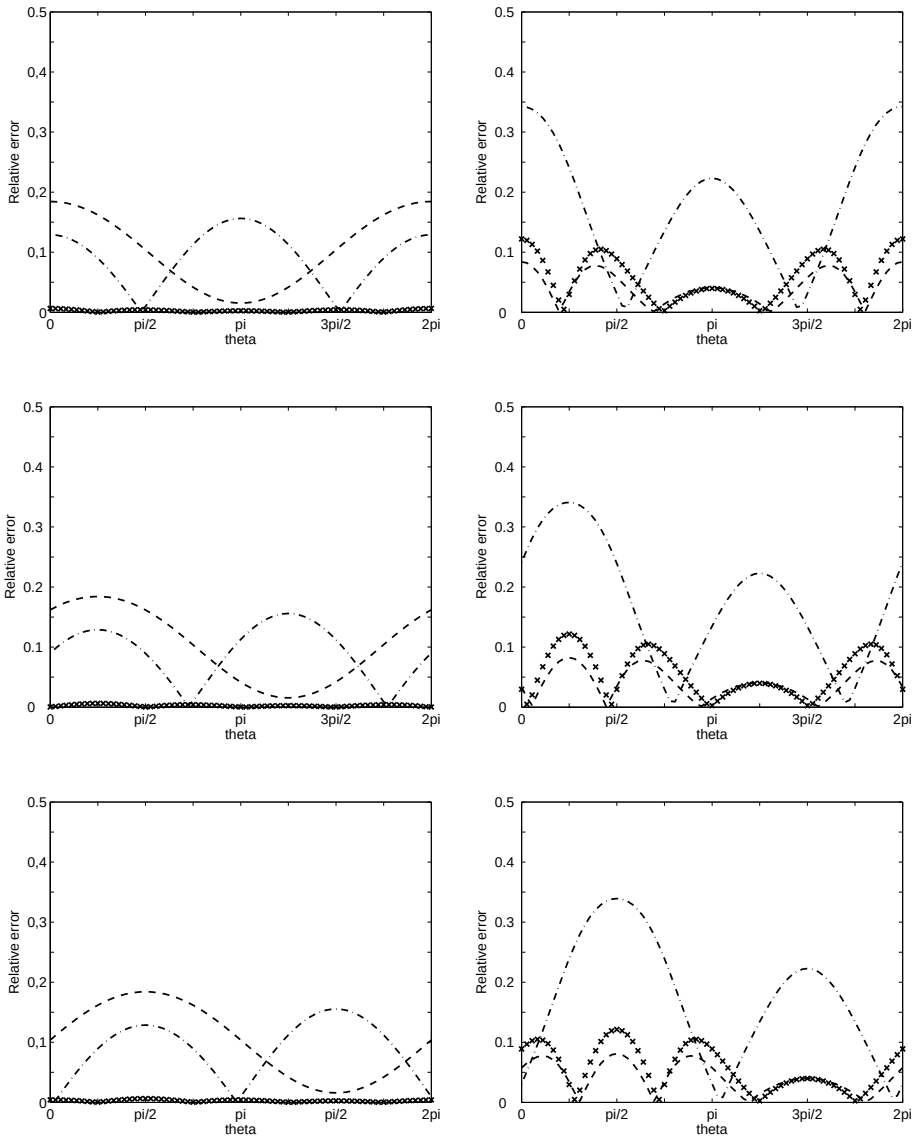

Figure 9: Relative error of the specific impedance for the DtN1 (dashed/dotted), the DtN2 (crossed), the BGT2 (dashed) for $ka = 0.1$ (left) and $ka = 1$ (right) for the incident angles $\theta_0 = 0$ (up), $\theta_0 = \frac{\pi}{4}$ (middle), $\theta_0 = \frac{\pi}{2}$ (down).

$e = 0.6$

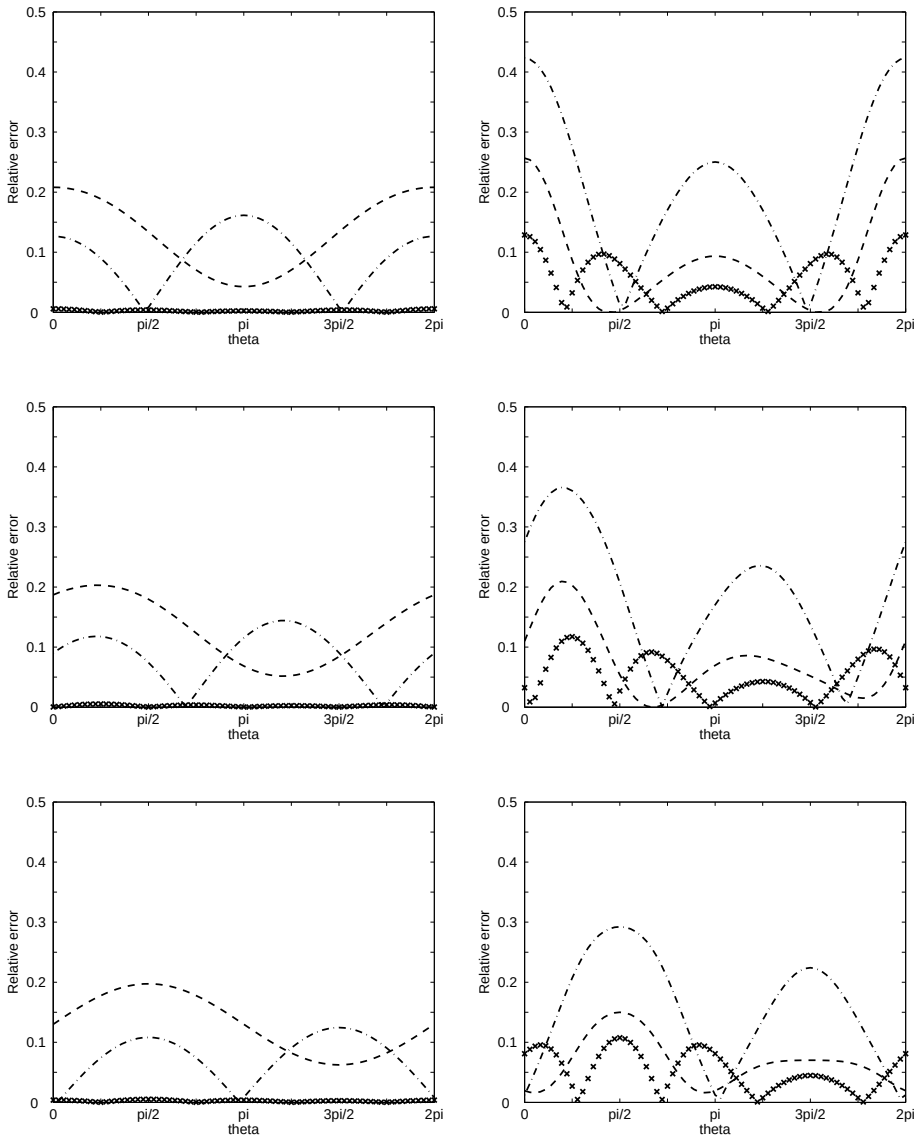

Figure 10: Relative error of the specific impedance for the DtN1 (dashed/dotted), the DtN2 (crossed), the BGT2 (dashed) for $ka = 0.1$ (left) and $ka = 1$ (right) for the incident angles $\theta_0 = 0$ (up), $\theta_0 = \frac{\pi}{4}$ (middle), $\theta_0 = \frac{\pi}{2}$ (down).

$e = 0.9$

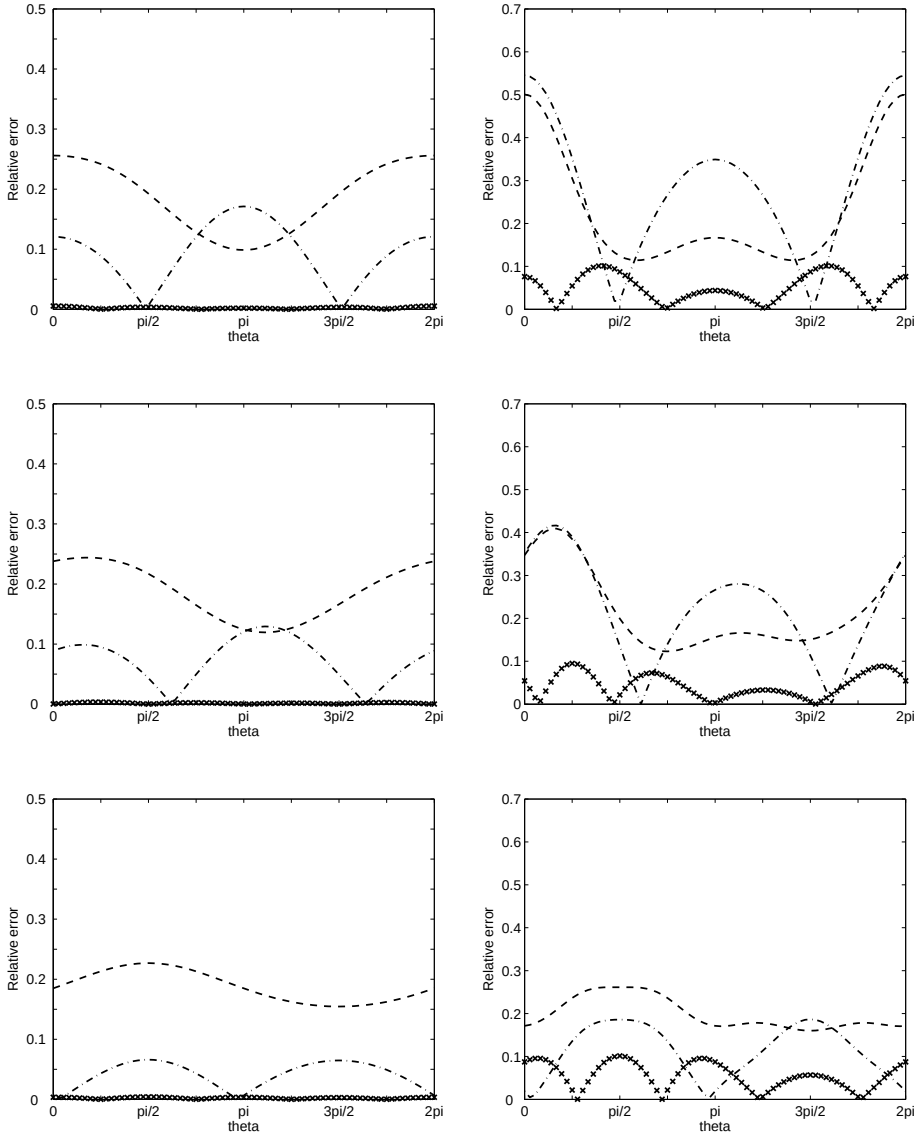

Figure 11: Relative error of the specific impedance for the DtN1 (dashed/dotted), the DtN2 (crossed), the BGT2 (dashed) for $ka = 0.1$ (left) and $ka = 1$ (right) for the incident angles $\theta_0 = 0$ (up), $\theta_0 = \frac{\pi}{4}$ (middle), $\theta_0 = \frac{\pi}{2}$ (down).

5 Conclusion

We have designed a new class of approximate local ABCs to be applied on elliptical-shaped exterior boundaries when solving acoustic scattering problems by elongated obstacles. These conditions are *exact* for the first radiation modes, they are easy to implement and to parallelize, and they preserve the local structure of the computational finite element scheme. The numerical investigation reveals that in the case of radiator problems, the DtN boundary conditions exhibit a significant loss of accuracy when computing higher mode, as expected from the analytical study. The situation is different when solving acoustic scattering problems. The analysis reveals that the second-order DtN2 boundary condition retains an excellent level of accuracy for low wavenumber values ka and for all eccentricity values e. This clearly demonstrates the superiority of the DtN2 boundary condition over the second-order BGT2 absorbing boundary condition, especially for eccentricity values $e \geq 0.6$. Hence, the new second-order absorbing boundary condition extends the range of satisfactory performance to all eccentricity values, which makes this absorbing boundary condition appropriate for very elongated elliptical-shaped boundaries.

Acknowledgements

The authors acknowledge the support by INRIA/CSUN Associate Team Program. Any opinions, findings, conclusions or recommendations expressed in this material are those of the authors and do not necessarily reflect the views of INRIA or CSUN.

References

[1] M. Abramovitz, I. Stegun, Handbook of Mathematical Functions with Formulas, Graphs and Mathematical Tables, Dover Publications, New York, 1972

[2] X. Antoine, Fast approximate computation of a time-harmonic scattered field using the on-surface radiation condition method, IMA J. Appl. Math., 66(1):83–110, 2001

[3] X. Antoine, Fast approximate computation of a time-harmonic scattered field using the On-Surface Radiation method, IMA J. Appl. Math., 66, 83-110, 2001

[4] A. Bayliss, M. Gunzberger, and E. Turkel, Boundary conditions for the numerical solution of elliptic equations in exterior regions, SIAM J. Appl. Math., 42 (2), pp. 430-451, 1982

[5] C. Flammer, Spheroidal Functions, Standford University Press, Standford, CA, 1957

[6] T. L. Geers, Doubly asymptotic approximations for transient motions of submerged structures, J. Acoust. Soc. Am., 64 (5), pp. 1500-1508, 1978

[7] T. L. Geers, Third-order doubly asymptotic approximations for computational acoustics, J. Comput. Acoust., 8 (1), pp. 101-120, 2000

[8] D. Givoli and J. B. Keller, Nonreflecting boundary conditions for elastic waves, Wave Motion, 12(3):261–279, 1990

[9] M. J. Grote, J. B. Keller, On nonreflecting boundary conditions, J. Comput. Phys., 122, 2, 231-243, 1995

[10] D. Givoli, Exact representations on artificial interfaces and applications in mechanics, AMR, 52(11):333–349, 1999

[11] I. Harari, Computational methods for Problems of Acoustics with Particular Reference to Exterior Domains, PhD thesis, Stanford university, May 1991

[12] I. Harari and T. J. R. Hughes, Analysis of continuous formulations underlying the computation of time-harmonic acoustics in exterior domains, Comput. Methods Appl. Mech. Engrg., 97(1):103–124, 1992

[13] I. Harari, R. Djellouli, Analytical study of the effect of wave number on the performance of local absorbing boundary conditions for acoustic scattering, Applied Numerical Mathematics, 50, 15-47, 2004

[14] J. B. Keller, D. Givoli, Exact nonreflecting boundary conditions, J. Comput. Phys., 82 (1), 172-192,1989

[15] G. A. Kriegsmann, A. Taflove, and K. R. Umashankar, A new formulation of electromagnetic wave scattering using an on-surface radiation boundarycondition approach, IEEE Trans. Antennas and Propagation 35 (2), 153–161, 1987

[16] R.C. Reiner, R. Djellouli, and I. Harari, The performance of local absorbing boundary conditions for acoustic scattering from elliptical shapes, Comput. Methods Appl. Mech. Engrg, 195, 3622-3665, 2006

[17] R.C. Reiner and R. Djellouli, Improvement of the performance of the BGT2 condition for low frequency acoustic scattering problems, Journal of Wave Motion, 43, pp. 406-424, 2006.

[18] A. Saint-Guirons, Construction et analyse de conditions aux limites absorbantes pour des problèmes de propagation d'ondes, Ph.D. thesis, (In Preparation).

[19] T. B. A. Senior, Scalar diffraction by a prolate spheroid at low frequencies, Canad. J. Phys. 38 (7) (1960) 1632-1641

[20] J.A. Stratton, Electromagnetic theory, McGraw-Hill, New York, 1941

[21] E. Turkel, Iterative methods for the exterior Helmholtz equation including absorbing boundary, conditions, In: Computational Methods for Acoustics Problems, F. Magoulès (ed.), Saxe-Coburg Publications (To Appear)

Contents

Unité de recherche INRIA Futurs
Parc Club Orsay Université - ZAC des Vignes
4, rue Jacques Monod - 91893 ORSAY Cedex (France)

Unité de recherche INRIA Lorraine : LORIA, Technopôle de Nancy-Brabois - Campus scientifique
615, rue du Jardin Botanique - BP 101 - 54602 Villers-lès-Nancy Cedex (France)
Unité de recherche INRIA Rennes : IRISA, Campus universitaire de Beaulieu - 35042 Rennes Cedex (France)
Unité de recherche INRIA Rhône-Alpes : 655, avenue de l'Europe - 38334 Montbonnot Saint-Ismier (France)
Unité de recherche INRIA Rocquencourt : Domaine de Voluceau - Rocquencourt - BP 105 - 78153 Le Chesnay Cedex (France)
Unité de recherche INRIA Sophia Antipolis : 2004, route des Lucioles - BP 93 - 06902 Sophia Antipolis Cedex (France)

Éditeur
INRIA - Domaine de Voluceau - Rocquencourt, BP 105 - 78153 Le Chesnay Cedex (France)
http://www.inria.fr
ISSN 0249-6399